



NASA Public Access

Author manuscript

Front Environ Sci. Author manuscript; available in PMC 2019 September 18.

Published in final edited form as:

Front Environ Sci. 2018 ; 6: . doi:10.3389/fenvs.2018.00085.

The Dawn of Geostationary Air Quality Monitoring: Case Studies from Seoul and Los Angeles

Laura Judd^{1,2,*}, Jassim Al-saadi¹, Lukas Valin³, R. Bradley Pierce⁴, Kai Yang⁵, Scott Janz⁶, Matt Kowalewski^{6,7}, James Szykman³, Martin Tiefengraber^{8,9}, Moritz Mueller^{8,9}

¹NASA Langley Research Center, Hampton, Virginia, USA

²NASA Postdoctoral Program, Hampton, Virginia, USA

³Environmental Protection Agency Office of Research & Development, Research Triangle Park, North Carolina, USA

⁴NOAA National Environmental Satellite Data and Information Service, Center for SaTellite Applications and Research, Madison, Wisconsin, USA

⁵Department of Atmospheric and Oceanic Science, University of Maryland College Park, College Park, Maryland, USA,

⁶NASA Goddard Space Flight Center, Greenbelt, Maryland, USA

⁷University Space Research Association, Columbia, Maryland, USA

⁸LuftBlick, Kreith, Austria

⁹Institute of Atmospheric and Cryospheric Sciences, University of Innsbruck, Innsbruck, Austria

*Correspondence: Laura Judd, laura.m.judd@nasa.gov.

⁸Author contributions

LJ, JA, and BP formulated the central research idea. LJ and JA drafted the manuscript. LJ led the processing and analysis of GeoTASO data. MT and MM processed the Pandora NO₂ retrievals and LV led Pandora data analysis. BP provided the modeled meteorology dataset and relevant processing scripts. KY provided OMPS NM data. JS was involved with Pandora measurements and maintenance in South Korea. SJ, MK, and JA participated in the flight planning and data gathering during GeoTASO flights in South Korea, with the addition of LJ in California. All authors provided input, suggestions, and edits to the manuscript.

⁶Conflict of Interest

The authors declare that the research was conducted in the absence of any commercial or financial relationships that could be construed as a potential conflict of interest.

⁹Data availability

- GeoTASO data can be provided upon request and will become publically available after June 2018 on the KORUS-AQ data archive (<https://www-air.larc.nasa.gov/cgi-bin/ArcView/korusaq?B200=1>) and the LMOS archive (<https://www-air.larc.nasa.gov/cgi-bin/ArcView/lmos>)
- Pandora data are available on data.pandonia.net
- OMPS data are available at <https://dx.doi.org/10.5067/N0XVLE2QAVR3>
- GFS and NAM meteorology are available at <http://nomads.ncep.noaa.gov/>
- SCAQMD hourly data is available <https://www.arb.ca.gov/aqmis2/metselect.php>, and higher temporal resolution is available upon request from SCAQMD.

¹⁰Publisher's Disclaimer:

Publisher's Disclaimer: The views, opinions, and findings contained in this report are those of the author(s) and should not be construed as an official National Oceanic and Atmospheric Administration, Environmental Protection Agency, or U.S. Government position, policy, or decision.

Abstract

With the near-future launch of geostationary pollution monitoring satellite instruments over North America, East Asia, and Europe, the air quality community is preparing for an integrated global atmospheric composition observing system at unprecedented spatial and temporal resolutions. One of the ways that NASA has supported this community preparation is through demonstration of future space-borne capabilities using the Geostationary Trace gas and Aerosol Sensor Optimization (GeoTASO) airborne instrument. This paper integrates repeated high-resolution maps from GeoTASO, ground-based Pandora spectrometers, and low Earth orbit measurements from the Ozone Mapping and Profiler Suite (OMPS), for case studies over two metropolitan areas: Seoul, South Korea on June 9th, 2016 and Los Angeles, California on June 27th, 2017. This dataset provides a unique opportunity to illustrate how geostationary air quality monitoring platforms and ground-based remote sensing networks will close the current spatiotemporal observation gap. GeoTASO observes large differences in diurnal behavior between these urban areas, with NO₂ accumulating within the Seoul Metropolitan Area through the day but NO₂ peaking in the morning and decreasing throughout the afternoon in the Los Angeles Basin. In both areas, the earliest morning maps exhibit spatial patterns similar to emission source areas (e.g., urbanized valleys, roadways, major airports). These spatial patterns change later in the day due to boundary layer dynamics, horizontal transport, and chemistry. The nominal resolution of GeoTASO is finer than will be obtained from geostationary platforms, but when NO₂ data over Los Angeles are up-scaled to the expected resolution of TEMPO, spatial features discussed are conserved. Pandora instruments installed in both metropolitan areas capture the diurnal patterns observed by GeoTASO, continuously and over longer time periods, and will play a critical role in validation of the next generation of satellite measurement.. These case studies demonstrate that different regions can have diverse diurnal patterns and that day-to-day variability due to meteorology or anthropogenic patterns such as weekday/weekend variations in emissions is large. Low Earth orbit measurements, despite their inability to capture the diurnal patterns at fine spatial resolution, will be essential for intercalibrating the geostationary radiances and cross-validating the geostationary retrievals in an integrated global observing system.

Keywords

NO₂; atmospheric composition; Pandora; GeoTASO; OMPS; air quality; satellite; geostationary

1 Introduction

The atmospheric chemistry community has long held a vision for an integrated observing system that provides continuous long-term information at the spatial and temporal resolutions adequate for monitoring air quality at local, regional, and global scales. This vision was first coherently expressed in the Integrated Global Observing Strategy (IGOS) Atmospheric Chemistry Theme Report over a decade ago (IGACO, 2004). While this vision is broadly similar to what has been accomplished in the global meteorological community, its implementation for atmospheric composition is still in its infancy. Satellite observations are an essential component, providing continuous coverage over large areas globally. Observation requirements relevant to air quality from satellites include temporal sampling at

approximately one-hour frequency and horizontal resolution on the order of 10 km (IGACO, 2004; Fishman et al., 2012). These temporal and spatial requirements can be met globally by using a constellation approach that combines multiple geostationary Earth orbit (GEO) platforms, which provide frequent observations over portions of the globe, with low Earth orbit (LEO) platforms, which provide global once-daily coverage (CEOS, 2011). Such a constellation strategy has been used for operational meteorological observations for decades.

Measurements of ultraviolet-visible (UV-VIS) radiation needed to perform atmospheric chemistry retrievals of ozone and its precursors have been made from platforms in LEO for the past 22 years beginning with the launch of the Global Ozone Monitoring Experiment (GOME) in 1996 (Burrows et al., 1998), and continuing with the launch of the Ozone Monitoring Instrument (OMI) in 2004 (Levelt et al., 2006), SCanning Imaging Absorption SpectroMeter for Atmospheric CHartographY (SCIAMACHY) in 2002 (Bovensmann et al., 1999), GOME-2 in 2006 and 2013 (Callies et al., 2000), the Ozone Mapping and Profiler Suite Nadir Mapper (OMPS NM) in 2011 and 2017 (Flynn et al., 2004, Yang et al., 2014), and the TROPOspheric Monitoring Instrument (TROPOMI) in 2017. These data have been useful for understanding global (e.g., Martin et al., 2003, Richter et al., 2005; Jaegle et al., 2005), regional (e.g., Duncan et al., 2014; Duncan et al., 2016; Travis et al., 2016) and local air quality (e.g., Valin et al., 2013; Zhu et al., 2017) over daily (e.g., Beirle et al., 2003; Valin et al., 2014; de Foy et al., 2016), seasonal (e.g., Jaegle et al. 2005, Russell et al., 2010), interannual, and decadal time periods (van der A et al., 2008; de Smedt et al. 2015). However, the relatively coarse spatial resolutions and single daily observation times have substantially limited these applications, particularly within the air quality management community which needs to be able to distinguish temporal profiles of emissions from different source sectors and identify specific physical processes to justify regulatory decisions.

Three GEO air quality missions are planned to be launched in the 2019–2023 period: Korea's Geostationary Environmental Monitoring Spectrometer (GEMS) observing East Asia (Kim et al., 2017), the United States' Tropospheric Emissions: Monitoring of Pollution (TEMPO) observing North America (Zoogman et al., 2017), and Europe's Sentinel-4 observing Europe (Ingmann et al., 2012), placing us on the cusp of a revolution in time-resolved air quality observations from space. Similar to LEO instruments, these missions each consist of imaging spectrometers measuring scattered light from the Earth's atmosphere in the UV-VIS wavelength range. Using molecular absorption features within this range, the column-integrated atmospheric abundances of certain trace gases and aerosols can be accurately retrieved. Target species relevant for air quality include ozone (O_3), nitrogen dioxide (NO_2), formaldehyde (HCHO), and sulfur dioxide (SO_2), as well as aerosol optical depth. Figure 1 shows the planned viewing regions for each GEO mission overlaid on an image of the June 2016–2017 average OMPS NM NO_2 column product (Yang et al., 2014). Unlike the single daily overpass and coarse footprint of legacy LEO missions (e.g., OMPS NM, 50 km \times 50 km, 13:30 LST), each GEO instrument will be capable of scanning its field of regard every hour at spatial resolutions of better than 10 km. Recently launched LEO instruments which are currently in check-out phase, TROPOMI and OMPS NM aboard NOAA-20, have footprints of 3.5 km \times 7 km and 17 km \times 17 km at nadir, respectively (van Geffen et al, 2017; L. Flynn, personal communication), providing global measurements with

sufficient spatial detail for cross-validating the three non-overlapping GEO components of the constellation.

LEO measurements play a critical role in the global atmospheric composition constellation by providing a means of intercalibrating and cross validating the GEO sensors and by providing observations outside the fields of regard of the GEO sensors, as shown by Figure 1. The importance of the LEO component of the Global Observing System for intercalibration of LEO and GEO radiances has been recognized by the WMO-sponsored Global Space-based Intercalibration System (GSICS, <http://gsics.wmo.int/>), which is responsible for operational intercalibration of satellite instruments. To expand capability beyond existing activities for sensors using visible and infrared wavelengths, GSICS has initiated a UV Subgroup that focuses on cross-calibration of ultraviolet sensors, including existing LEO and future GEO instruments. Harmonizing atmospheric composition retrievals among LEO and GEO sensors is also necessary for effective utilization of the LEO and GEO measurements.

The spatial (< 10 km) and temporal (hourly) requirements for air quality satellites have largely been determined by the desire to resolve the processes affecting the emissions, lifetime and transport of tropospheric NO₂ (e.g., Beirle et al., 2011; Valin et al., 2011a; 2013; de Foy et al., 2015) because of its fundamental role in the formation of tropospheric ozone and particulate matter. There have been a variety of approaches for validating NO₂ products retrieved from LEO platforms (e.g., Boersma et al., 2008; Bucseles et al., 2008, 2013; Irie et al., 2008; Lamsal et al., 2010; Russell et al., 2011; Travis et al., 2016). These works have identified and addressed gaps in the understanding of NO₂ retrievals, including methods for subtracting stratospheric NO₂ column contributions, a priori vertical profile deviations between urban and rural settings, and surface reflectance variations (e.g., Zhou et al., 2010; Russell et al., 2011). The additional retrieval assumptions relevant to GEO observations, for example changes in the a priori vertical profile from morning to afternoon under different solar angles or downwind of a large point source such as a power plant, are only beginning to be assessed.

To begin addressing the spatial and temporal challenges associated with GEO measurements prior to launch, NASA funded the development of the suborbital Geostationary Trace gas and Aerosol Sensor Optimization instrument (GeoTASO, Leitch et al., 2014, Nowlan et al., 2016) and has deployed it during recent field experiments that also included networks of ground-based UV-VIS solar spectrometers (Pandora, Herman et al., 2009; 2015). Analogous to how the LEO observations are a transfer standard between the GEO domains, the airborne observations are a transfer standard between the spatial scales of the surface-based validation instruments (i.e. Pandora) and satellite observations. Here we use GeoTASO and Pandora datasets collected as part of the KORUS-AQ study in Seoul, South Korea during spring 2016 and as part of the NASA Student Airborne Research Program in Los Angeles, California, USA in summer 2017 to demonstrate the spatial and temporal richness of the in anticipation of what will be routinely provided in the near-future GEO-based measurements. We frame this discussion in the context of LEO-based OMPS NM NO₂ column measurements to highlight both the spatial and temporal limitations of past datasets but also to demonstrate how LEO-platforms will continue to provide important global context to

GEO-based sensors. Although field campaigns cover limited areas and time periods, these measurements are providing a first taste of the air quality observations that will be provided by scheduled GEO missions at an hourly timescale.

2 Data

2.1 GeoTASO

GeoTASO is an aircraft-based UV-VIS hyperspectral imaging spectrometer built by Ball Aerospace (Leitch et al., 2014). It is being used to test air quality remote sensing retrievals for the future GEO observations from TEMPO, GEMS, and Sentinel-4. The instrument was first deployed during the NASA DISCOVER-AQ study in Houston, Texas in September 2013 (Nowlan et al., 2016). The data presented here were obtained by operating GeoTASO on the NASA LaRC's UC-12B aircraft at a nominal altitude of 8.5 km. GeoTASO has two 2-dimensional CCD detectors, gathering spectral data in the visible (VIS) wavelengths (410–690 nm) and in the UV wavelengths (300–380 nm). NO₂ retrievals only use data from the VIS detector, which records spectra in one dimension (1056 pixels) and cross-track spatial data in the second dimension (1033 pixels). The spectral integration time is fixed at 250 ms while traveling at ground speeds of approximately 100 m/s. GeoTASO's nadir cross-track field of view is 45° providing approximately 7 km of cross-track coverage at altitude. Prior to the NO₂ retrieval, spectra are binned spatially to approximately 250 m × 250 m to increase the signal-to-noise ratio. Gapless maps were created to simulate GEO observations by flying a series of parallel flight lines spaced such that there was a small overlap between the adjacent swaths, taking into consideration GeoTASO's 45° field of view and nominal flight altitude. Flight plans were developed to cover areas of 4,000–8,000 km² so that as many as four repeat measurements could be captured each day. A single traverse of this pattern across an area is referred to as a raster pattern.

Spectra from 435–460nm, blue-visible light, are used to retrieve NO₂ differential slant columns (DSCs) via Differential Optical Absorption Spectroscopy (DOAS). An open-source software developed at the Royal Belgian Institute for Space Aeronomy called QDOAS (Danckaert et al., 2016) is used to compute DSCs relative to an unpolluted reference spectrum taken in flight. The resulting DSC retrievals represent the total amount of NO₂ molecular absorption along the slant path of the light relative to what was present in the unpolluted reference measurement. For this study, the native resolution (250 m × 250 m) DSCs are averaged to a spatial resolution of 750 m × 750 m by co-adding three adjacent along-track and three adjacent across-track pixels, which is still finer than any proposed GEO or LEO satellite. This averaging decreases the average DSC error from 1.6×10^{15} molecules cm⁻² to approximately 5×10^{14} molecules cm⁻² and decreases the noise observed over the area of the reference spectrum (the zero baseline for these measurements) by over 50%.

DSCs are typically converted to vertical columns using a calculated air mass factor (AMF) (Palmer et al., 2001; Lamsal et al., 2017). For a non-scattering atmosphere, the AMF simply reflects a geometric correction of the slant path of light relative to a vertical path through the atmosphere. However, because light traveling through Earth's atmosphere is heavily influenced by scattering, AMF calculations require a radiative transfer model that

incorporates a priori assumptions about the vertical distribution of relevant trace gases (NO_2), surface albedo, pressure, and aerosols, in addition to solar and viewing geometry. Ideally, the ancillary information used to calculate AMFs should be at a spatial resolution similar to or better than the DSC measurements to avoid introducing biases and artifacts (Russell et al., 2011). Many datasets necessary for the AMF calculations do not yet exist at the sub-kilometer spatial scales at which we are retrieving NO_2 and biases due to coarse a priori assumptions have not yet been evaluated at this sub-kilometer spatial scale. For the early results shown in this study, fine spatial resolution AMFs have not yet been calculated, therefore DSC values are shown to avoid potentially introducing spatiotemporal artifacts associated with coarse AMF calculation. This simplification does not fundamentally alter the conclusions of this study, as the variability of previously calculated AMFs for GeoTASO (Nowlan et al., 2016) is much smaller than the spatiotemporal patterns observed in this study.

The stratospheric contribution of NO_2 to the total column is small ($\sim 3 \times 10^{15}$ molecules cm^{-2}) and spatially uniform relative to the tropospheric DSCs observed over Los Angeles and Seoul. The temporal variation in this contribution is also small ($\sim 1 \times 10^{14}$ molecules $\text{cm}^{-2} \text{h}^{-1}$) (Sussmann et al., 2005). When retrieving DSCs from GeoTASO, the contribution of stratospheric NO_2 is observed similarly in the clean reference spectrum measurement as in all measurements, and thus is implicitly subtracted in the fitting procedure. However, time difference between the reference and retrieved observation introduces a bias in the DSCs due to the changing solar geometry altering the path length of the solar beam through the stratospheric NO_2 layer. This time-dependent bias in the stratospheric NO_2 is estimated and a correction is applied to results shown here using the solar geometry and the stratospheric NO_2 vertical column observed from OMPS NM aboard Suomi NPP (Yang et al., 2014) on the day of observation over the region of the flight.

The urban areas in this study were mapped 3 to 4 times throughout one day to simulate how the magnitude and spatial distribution varies diurnally at unprecedented spatial resolutions for each location. In Korea, GeoTASO data were analyzed between longitudes of 126.4°E and 127.4°E and latitudes of 37.2°N and 37.7°N to exclude areas outside of the Seoul Metropolitan Area (SMA). Similarly, data over the Los Angeles (LA) Basin were analyzed between longitudes of -118.5°W and -117.4°W and latitudes of 33.7°N and 34.165°N to restrict data from outside the Basin.

2.2 Pandora spectrometer

In an effort to provide cost-effective methods for validating space-based UV-VIS trace gas measurements, including those from GEO, NASA and ESA are collaborating on a global network of ground-based Pandora Solar and sky-scanning spectrometers developed at NASA GSFC (Herman et al., 2009). Pandora spectrometers are capable of retrieving accurate and precise vertical columns of NO_2 using a direct-sun DOAS technique (Herman et al., 2009). Pandora instruments are operated continuously to retrieve an NO_2 column approximately every 90 seconds during daylight hours, whenever the path between the surface and the sun is cloud-free. These measurements are total NO_2 column with no differentiation of stratospheric or tropospheric NO_2 contributions, but as discussed in section 2.1, stratospheric

contributions are relatively small and not variable over LA and Seoul. Data from these instruments have been used to assess space- and aircraft- based retrievals of NO₂ columns (Flynn et al., 2014; Nowlan et al., 2016; Goldberg et al., 2017), as well as to study the spatiotemporal variability of trace gases in urban environments (Tzortziou et al., 2015) and column-to-surface relationships and their relation to boundary layer depth (Flynn et al., 2014; Knepp et al., 2013). Further understanding the effects of boundary layer depth on air quality has been identified as a ‘most important’ objective by the National Academy of Sciences’ most recent Decadal Survey (2017–2027) (National Academies of Sciences, Engineering, and Medicine, 2018).

This study shows NO₂ data from three Pandoras in the SMA from May 5th–June 15th, 2016 (Yonsei, Olympic Park and Mount Taehwa) and six Pandoras within the LA Basin from June 15th–July 15th 2017 (UCLA, LA Main Street, Pico Rivera, CalTech, Fontana, and Ontario). For each site, one-hour averages are calculated for analysis after the data are filtered according to recommended data quality criteria (vertical column error of less than 2.69×10^{14} molecules cm⁻² and normalized RMS less than 0.005). Each hourly average requires at least 5 valid observations within the hour. Longer term diurnal averages (total, weekend, weekday) also calculated for analysis require over 40 valid observations per hour.

2.3 Ozone Mapping and Profiler Suite Nadir Mapper (OMPS NM)

Data from the OMPS NM hyperspectral UV instrument aboard Suomi-NPP are used to demonstrate legacy LEO measurement capability and to illustrate plans for incorporation of recently launched (TROPOMI) and future LEO missions into the air quality observing constellation. While OMI data have higher spatial resolution than OMPS NM, OMI was not operational during part of the time period of this study. OMPS NM instruments are aboard Suomi-NPP launched in 2011 and JPSS-1 (now NOAA-20) launched in 2017. NO₂ is retrieved using an iterative spectral fitting algorithm at a nadir resolution of 50 km × 50 km (2500 km²) (Yang et al., 2014), which will be further improved to 17 km × 17 km (289 km²) for OMPS NM aboard NOAA-20 (L. Flynn, personal communication). OMPS NM NO₂ columns are also separated into their tropospheric and stratospheric components. The measurement precision of tropospheric NO₂ vertical column is estimated to be 3×10^{14} molecules cm⁻² (Yang et al., 2014). For this analysis, both tropospheric and stratospheric columns are used from the instrument aboard Suomi-NPP, with the latter helping correct the offset in GeoTASO’s DSCs due to the stratospheric NO₂ layer as described in section 2.1. Data from OMPS NM are filtered for cloud fractions greater than 25%.

3 Results and discussion

To demonstrate the capability and limitations of currently available data, Figure 2 shows single overpass and monthly-averaged OMPS NM NO₂ column measurements over South Korea and California. On June 9, 2016, the OMPS NM nadir overpass was to the west of the Seoul Metropolitan Area (SMA). Because of the viewing geometry and the curvature of the Earth, the OMPS NM off-nadir detector elements that view the SMA cover twice as much surface area as those at nadir (nominally 50 km × 50 km) on this day (Figure 2a). On the other hand, the OMPS NM nadir overpass was directly over Southern California on June

27th, 2017 (Figure 2b), such that OMPS NM was able to measure the tropospheric NO₂ column over LA near its finest spatial resolution.

LEO observations can be refined spatially by ‘oversampling’ over a longer temporal range, as the orbital track varies day-to-day leading to variable spatial sampling (e.g., the edge of swath over Korea on June 9th, 2016 vs. the nadir observations over Los Angeles from June 27th, 2017). This technique has been applied to trace-gas retrievals from imaging spectrometers, like OMI, for NO₂, HCHO, and SO₂ data to identify and investigate pollution emitting sources, their average plume extent, and emission rates (deFoy et al., 2009; Russell et al., 2010; McLinden et al. 2012; Zhu et al., 2014). Figure 2c and d show the 0.25° × 0.25° (approximately 20 km × 30 km at 35°N) monthly average created by oversampling OMPS NM NO₂ data for June 2016 over South Korea (Figure 2c) and June 2017 over California (Figure 2d). Here, the OMPS NM average measurements show that NO₂ columns are locally maximum over Seoul and Los Angeles. By providing the means to distinguish sources, long-term trends can be used to evaluate the changes of emissions driven by regulatory programs (Kim et al., 2006), technological controls (e.g., Russell et al., 2012) and economic activity (e.g., Russell et al., 2012; de Foy et al., 2016; Duncan et al., 2016). Whether considering daily measurements or analysis of long term monthly averages, instruments like OMPS NM provide a well-characterized, quantitatively stable measurement reflecting a balance of NO₂ emissions and removal at spatial scales of ~25 km, with some limited information on pollutant transport (e.g., Beirle et al., 2011; Valin et al., 2013; 2014; de Foy et al., 2016). As such, the measurements available from the past have not been sufficient to address the more pressing air quality management needs: the ability to distinguish sources within urban airsheds, characterization of local mesoscale flow patterns on pollutant transport, quantification of NO₂ removal mechanisms (e.g., Valin et al., 2013), or better characterization of photochemical ozone production to NO_x (NO + NO₂) or VOC control strategies (e.g., Martin et al., 2004; Duncan et al., 2010; Jin et al., 2017; Schroeder et al. 2017).

The LEO-based data in Figures 1 and 2 represent the standard measurement that has been available to observe pollutants globally from space-based platforms for more than two decades. While finer scale global LEO data will soon be available with the addition of TROPOMI and NOAA-20 OMPS NM, the following two case studies demonstrate the information that will be gained in adding temporally resolved GEO observations to this global observing system by focusing on GeoTASO and Pandora measurements within the Seoul Metropolitan Area (SMA) and the Los Angeles (LA) Basin in June 2016 and 2017, respectively. Figure 3 shows maps of each metropolitan area discussed in these case studies. The white polygons encompass the area observed by GeoTASO, white stars and labels are Pandora locations, red/blue lines are major roadways (SEDAC, 2013), and icons and regions labeled in yellow are discussed in Section 3.1 and 3.2. Areas of elevated terrain appear darker than the surrounding valleys and are typically free of strong emission sources. Densely urbanized areas within the valleys appear greyer in color. Using this map as a reference will help guide the discussion below.

3.1 Case study 1: Seoul Metropolitan Area, South Korea

The first execution of diurnal mapping over an urban area with GeoTASO was during the DISCOVER-AQ Front Range field study in summer 2014 (Crawford, et al., 2016). This same strategy was used more extensively during the KORUS-AQ field study in spring 2016 (<https://www-air.larc.nasa.gov/missions/korus-aq/>). Figure 4 shows maps of NO₂ DSC obtained by GeoTASO on June 9, 2016, at 4 different times of day between 08:00–18:00 LT over the Seoul Metropolitan Area (SMA). Each of the 4 rasters covers an area of approximately 40 km × 70 km in approximately two hours. This is also the approximate area of a single nadir OMPS NM pixel (Figure 2). Overlaid in panels a and c in Figure 4 are wind vectors averaged over the lowest 500 m agl from the full spectral resolution (~13-km) Global Data Assimilation System (GDAS) analyses for 00:00 UTC (09:00 LT) and 06:00 UTC (15:00 LT), respectively (Kleist and Ide, 2015a, 2015b). Output, archived at standard 6-hour intervals, is not available during the other two rasters.

Figure 5 shows percentile distributions of NO₂ DSCs for each SMA raster shown in Figure 4. Over the SMA area on this day, NO₂ pollution is at its minimum in the morning then increases and becomes more variable throughout the day, demonstrating the accumulation of NO₂ at a rate faster than its removal. The area median more than doubles from 20×10^{15} molecules cm⁻² to 49×10^{15} molecules cm⁻² over the course of the day with the interquartile range (representing the variability) expanding as well. There is not a significant change in the median from late morning to mid-afternoon, however the distribution is skewed upwards with the 75th percentile reaching 58×10^{15} molecules cm⁻² for Raster 3. Raster 4 exhibits the largest magnitude and variability of NO₂ columns on June 9th with the median DSCs approaching 50×10^{15} molecules cm⁻² and an interquartile range of 44×10^{15} molecules cm⁻². Maximum DSCs observed over the SMA during this day, up to 120×10^{15} molecules cm⁻² and well exceeding the 95th percentile, occurred during Rasters 3 and 4.

During the morning (Rasters 1 and 2), distinct patterns are apparent with maximum NO₂ DSCs over urbanized valleys and minimums located directly over elevated terrain. The western minima located south-southeast of Incheon is not due to elevated terrain, but instead due to the lack of large emission sources within this rural farmland region. The largest DSCs in the morning coincide with the areas with the largest temporal growth between Raster 1 and Raster 2, including Incheon, south central Seoul, and Suwon, where the DSCs grow to a magnitude outside of the interquartile range. These are areas with dense urbanization shown in Figure 3 and are likely the areas with the largest emissions in this domain.

The morning patterns reflect emission sources (i.e. roads and urban centers) that are confined spatially. In comparison, the spatial distribution of NO₂ DSCs in the afternoon changes dramatically. The boundary layer grows through the day due to surface heating, and from Raster 2 to Raster 3 grows deep enough to encompass the surrounding terrain. By the afternoon it appears the mixed layer is deep enough and advection is fast enough that the spatial pattern of NO₂ columns no longer reflects the pattern of emission sources. While muted in a deeper afternoon mixed layer, the terrain influence on the spatial pattern of NO₂ columns is still visible in Raster 4, where there is a local minimum in middle of the SMA plume with a magnitude of $\sim 70 \times 10^{15}$ molecules cm⁻² near Mt. Gwanaksan (green triangle in Figure 3 and 4). Over the nearby valley (5 km west), NO₂ DSC values are 20×10^{15}

molecules cm^{-2} larger. Assuming that the mixed layer height is independent of terrain variations, the 20×10^{15} molecules cm^{-2} would equate to an average mixing ratio of 20 ppbv within the 400 m between the valley floor and the elevated terrain (assuming a temperature of 300 K and surface pressure of 1000hPa). This mixing ratio estimate of 20 ppbv compares well with the mixing ratios measured nearby by NCAR's 4-channel chemiluminescence instrument aboard the NASA DC-8 aircraft on this afternoon during a KORUS-AQ flight (not shown). In such situations, local minima in column amounts may not correspond to local minima in surface concentrations. GEO observations, Pandora measurements, and routine air quality monitoring networks will begin to resolve some of these differences in areas with complex terrain and provide translation to similar locations without surface monitoring.

While NO_2 over the SMA generally accumulates throughout the day, this is not true for all locations within the region. On June 9th, 2016, winds from the GDAS analyses near the SMA shift from weak northerly flow in the morning (00:00 UTC – 09:00 LT) to stronger westerly flow during the afternoon (06:00 UTC – 15:00 LT). The spatial pattern over the SMA does not change from Raster 1 to Raster 2. However, during the afternoon there is a shift progressively to the east between Rasters 3 and 4, indicative of horizontal transport. This is most apparent by observing the edges of the SMA NO_2 DSC plume, such as at Incheon where there is significant growth between Rasters 1 and 2, but then decay and/or extension toward the east during the afternoon rasters. Additionally, it takes approximately two hours to cover the area of the domain in each Rasters. In Raster 3, the spatial offsets of DSCs between successive overpasses (ranging from 15–30 minutes) between Incheon and south Seoul is likely caused by advection of the plume between Raster line samples. On the eastern side of the domain, the Mount Taehwa area is relatively unpolluted during Rasters 1 and 2, but between Raster 3 and Raster 4, NO_2 DSCs increase and are consistent with what would be expected from the advection of the SMA plume to southeast based on the 15:00 LT winds.

As part of efforts to demonstrate GEO validation plans, Pandora instruments provided direct sun vertical column NO_2 measurements that are complementary to the GeoTASO backscatter DSCs at three sites in the region (Figure 6). The selected sites cover a range of air quality conditions across the SMA, spanning the domain of GeoTASO observations from the northwest (Yonsei is just outside the raster domain due to airspace restrictions) to the east-southeast over Olympic Park and Mount Taehwa another 40 km southeast (stars in Figures 2 and 4). Grey lines in Figure 6 show the hourly-averaged diurnal pattern for all days between May 5th and June 15th, 2016, with the day of the GeoTASO observations, June 9th, highlighted in red. On June 9, 2016, the observations at these sites are broadly consistent with the NO_2 column growth and transport patterns observed by GeoTASO; NO_2 columns are large and growing over low-lying population centers during the morning hours (e.g., Yonsei and Olympic Park) followed by transport to the southeast, such that columns diminish over Yonsei in the early afternoon while growing over Olympic Park briefly (also seen in Raster 3 from GeoTASO: Figure 4c) before finally diminishing over Olympic Park and growing over Taehwa in the late afternoon. At Yonsei University, Pandora measurements were made from the top of a campus building (180 m MSL, ~130 m AGL). As a result, observations at Yonsei University are biased low at all times of the day, especially in the

morning hours, when the unsampled portion of the boundary layer (130 m) is a larger component of the typically shallower NO₂ mixing depth. A similar bias has been observed and quantified for previous Pandora measurements in Houston using coincident NO₂ in situ measurements (Nowlan et al., 2016; Judd, 2016), however this potential bias does not change the larger conclusions made here.

June 9th, 2016 was the only day that GeoTASO was used to acquire observations at 4 different times throughout the day. However, the Pandora measurements show large day-to-day variations of NO₂ column at these sites across the SMA (Figure 6, gray lines), particularly over the urban sites of Yonsei and Olympic Park, but also over the rural Mount Taehwa site, downwind of Seoul. The hourly and daily variations of NO₂ column can provide important constraints on transport models, particularly when influences from local mountain and land-ocean circulations are challenging to accurately simulate. The hourly values from Figure 6 are also averaged to calculate the weekday diurnal average in solid black and weekend average in dashed black. At all sites, the weekend column densities are lower than those during the weekdays, highlighting the influence of anthropogenic activity on air quality. The longer-term averages of the NO₂ column reveal important information on chemical transport, but primarily reveal important lessons for understanding the chemical mass balance of NO₂ emissions and loss, or insights on the importance of sources of pollutant emissions that are known to have a day-of-week variation (e.g., Beirle et al., 2003; Harley et al., 2005; Valin et al., 2014).

The magnitude of NO₂ observed in the most polluted regions of the SMA by both Pandora and GeoTASO is over an order of magnitude larger than observed by OMPS NM (Figure 3). The LEO observations roughly coincide with the time of Raster 3 in the SMA. At Olympic Park at this time, Pandora and GeoTASO both measured spikes in the local NO₂ column at the same order of magnitude ($70\text{--}80 \times 10^{15}$ molecules cm⁻²) and the SMA as a whole had a median of 33×10^{15} molecules cm⁻². The order of magnitude discrepancy between the finer scale measurements (GeoTASO and Pandora) and the coarse LEO observations (OMPS NM) reflect spatial averaging of over an area that also includes less NO₂-polluted air. The SMA is observed by four OMPS NM pixels, each averaging only a fraction of the enhanced NO₂ columns over the SMA with a larger area of background NO₂ columns. Only moderate enhancements ($\sim 3 \times 10^{15}$ molecule cm⁻²) are observed over Seoul by the $\sim 20,000$ km² covered by the 4 OMPS NM pixels. Looking at the oversampled monthly averaged data (Figure 2c), the spatial patterns correlate better with those observed by GeoTASO observations with a peak centered over the SMA region. Over this month there are fewer polluted days than the case shown on June 9th, as shown by the Pandora measurements in Figure 6, resulting in a smaller magnitude of NO₂ over the SMA on the month time-scale vs. the afternoon sample from Raster 3. Comparisons of OMPS NM data (50 km × 50 km) with OMI data (24 km × 13 km) (Yang et al., 2014) and OMI operational products with super-zoom OMI data (~ 7 km × 13 km; Valin et al., 2011b) confirm that neither OMPS NM nor OMI operational footprints are sufficient to resolve the small-scale NO₂ spatial variations over localized sources. Due to the nature of NO₂ emissions and its short atmospheric lifetime, air quality applications require that the variability of NO₂ columns are spatially resolved (e.g., Cohan et al., 2006; Valin et al., 2011a), a capability anticipated from future LEO (TROPOMI: 3.5 km × 7 km) and GEO platforms.

3.2 Case Study 2: Los Angeles, California

Figure 7 shows NO₂ DSC maps obtained over the LA Basin at three different times on June 27th, 2017 capturing the morning, mid-day, and late afternoon periods. The left column shows the 750 m × 750 m resolution DSCs from GeoTASO and the right column shows a product that is co-added to 3 km × 3 km to emulate a sampling footprint that is more comparable to what is anticipated from GEO. The area of this raster spans approximately 50 km × 50 km in the southern half and approximately 115 km east-to-west on the northern side of the Basin. Overlaid are boundary layer averaged wind vectors from the North American Model (NAM)-CONUS 3 km nest (Janjic and Gall, 2012) from 16:00 UTC (09:00 LT) on Raster 1, 20:00 UTC (13:00 LT) on Raster 2, and 00:00 UTC (17:00 LT) for Raster 3. Figure 8 shows percentile distributions of NO₂ DSCs for each LA Raster at the 750 m resolution (the left column of Figure 7). Unlike over the SMA, maximum NO₂ columns are observed in the morning, with a median NO₂ DSC over the LA Basin of 12.5×10^{15} molecules cm⁻² during Raster 1. Notably, this value is lower than the minimum median observed over the SMA during any of those four rasters. The median value decreases approximately 50% between the morning and late afternoon (Raster 1 vs. Raster 3) in the LA Basin. The opposite diurnal pattern observed by GeoTASO over Seoul and Los Angeles may indicate more prevalent mid-day sources in Seoul relative to Los Angeles, differing chemistry regimes, or perhaps just a difference in transport patterns during the case study periods. With GEO platforms providing more data to test these hypotheses over many more urban areas, we anticipate exciting opportunities for future air quality research.

Similar to the SMA example, the winds are relatively light in the morning and the spatial distribution of NO₂ appears to mimic the distribution of emission sources. During Raster 1, enhancements that likely reflect mobile emission sources are located over freeways (i.e. I10, I5, and CA60: blue outlined roads in Figure 3) with the largest enhancements over downtown Los Angeles (just west of LA Main Street) where many of these freeways intersect and traffic congestion could lead to local emission enhancements. An additional maximum is observed over LAX Airport on the coast (airplane icon in Figure 3), a large NO_x emission source. The lowest columns measured coincide with areas of elevated terrain, such as the hills west of Long Beach, and areas of the Santa Ana mountains.

On the western side of the Basin during Raster 2, GeoTASO observes a line of high NO₂ DSCs, mimicking a frontal structure extending north-to-south from Glendale down to Long Beach, peaking near downtown Los Angeles. At the same time, the hot spot over LAX airport during Raster 1 is now more diffuse with a plume-like structure extending to the east, indicative of horizontal transport inland. With Los Angeles's location on the Pacific Coast, the area is often influenced by mesoscale land/water circulations (sea breezes) due to unequal heating over the land and water, which could result in westerly transport of pollution within the LA Basin during the daytime. Figure 9 illustrates the role of sea breeze transport on this day. Figure 9a shows contoured 2-meter relative humidity (RH) and boundary layer averaged wind vectors from the NAM-CONUS 3-km nest over the western half of the LA Basin at 20:00 UTC (13:00LT: the midpoint of Raster 2). On this map, the largest gradient in relative humidity and shift in wind vectors occurs around the 40% relative humidity contour indicating the boundary between the land and marine air masses (i.e. the

sea breeze front). The 40% contours from 19:00, 20:00, and 21:00 UTC are overlaid on the GeoTASO NO₂ DSCs from Raster 2 in Figure 9b to indicate the movement of the sea breeze front during Raster 2 in relation to the NO₂ feature observed during this time. These modeled results are similar in timing to the observed sea breeze arrival at the South Coast Air Quality Monitoring District's LA Main Street monitoring location, which saw an air mass transition at 13:30 LT with a slow increase in westerly wind speed and a 10% increase in RH. The edge of the peninsula to the west of Long Beach has hilly terrain that acts as a barrier to the penetrating sea breeze front, and due to the directional orientation of the coastline in this area, there are two different sea breeze fronts pushing inland and converging around the Long Beach area. The spatial structure of NO₂ during Raster 2 mimics the shape of the sea breeze front that is pushing inland, suggesting that this front is advecting the pollution that was along the coast to the east as the sea breeze progresses inland through the afternoon. In fact, it appears that NO₂ is trapped within the convergence zone between the two sea breeze fronts in the southern end of the Raster. The influence of air mass convergence on pollution build up has been observed in other coastal regions, such as in Houston, Texas, where synoptically driven offshore flow can converge with the sea breeze front allowing for the buildup of pollution within its convergence zone and causing poor air quality (Banta et al., 2005). Although less defined, this linear NO₂ feature within the continued presence of the convergence zone also appears in Raster 3 (Figure 7e) slightly further to the east, demonstrating the influence of this convergence zone over the duration of the afternoon.

The appearance of enhanced NO₂ during Raster 3 between downtown Los Angeles and the Inland Empire coincides with an area of enhancement also observed during the morning flight. It is impossible to tell from the available data in this study whether this enhancement is due to continued sea breeze transport or the result of increased local emissions during the late afternoon, but as a whole, these datasets demonstrate the complexity of the spatial distribution of NO₂ in a coastal urban metropolitan surrounded by complex terrain.

To provide an initial assessment of the data that will be routinely available from GEO observations, the Los Angeles data are binned up to 9 km² (expected nadir areal resolution of TEMPO: Zoogman et al., 2017) by averaging the data into 3 km × 3 km pixel bins (Figure 7 right). While the signatures are muted due to spatial averaging, the features discussed in the preceding paragraphs remain spatially distinct, demonstrating how GEO observations from TEMPO are expected to address salient air quality questions, even in a coastal region with complex terrain, mesoscale circulations, and temporal emission patterns.

Figure 10 is the same format as Figure 6, but for the 6 Pandoras installed in the Los Angeles Basin showing data between the dates of June 15th and July 15th, 2017. As is the case over Seoul, Pandora NO₂ vertical column measurements in the LA Basin on June 27th, 2017 (Figure 10: red lines) are broadly consistent with the NO₂ column growth and transport patterns observed by GeoTASO, most notably the early afternoon peak at LA Main Street coinciding with the sea breeze front arrival on this day. In Los Angeles, unlike Seoul, NO₂ columns observed by Pandora spectrometers are generally at a maximum in the mid-morning hours and decrease in the early afternoon hours on weekdays. Over coastal and downtown Los Angeles sites (UCLA, LA Main Street), NO₂ columns continue to decrease

or remain steady in the late afternoon hours whereas NO₂ columns grow at Pico Rivera, Ontario, and Fontana, reflecting the inland transport of cleaner air at the coast and more polluted air at the downwind sites in the presence of westerly prevailing winds.

While the overlying diurnal features are apparent on many days (e.g. the morning peak in NO₂ at most sites), day-to-day variability in Pandora data (Figure 10: grey lines) shows significant deviation from the average patterns. For example, the sea breeze front that shows a distinct maximum over LA Main Street on June 27th only occurs on a handful of other days that month. CalTech is also different from the other sites in that its NO₂ peak is around midday. Similar to Taehwa, CalTech is not a primary NO₂ source area, but instead a potential receptor to Los Angeles's early morning emissions under the right transport conditions (not seen on June 27th). Additionally, CalTech is approximately 250 m asl (or about 150 m higher than the LA Main Street site) and another midday contributor there may be mixing from lower-lying areas to the elevation sampled by the Pandora as the mixed layer grows throughout the day. Like Seoul, NO₂ columns are smaller at all sites on the weekend (Saturday-Sunday) than during the week (Monday-Friday), with a few sites exhibiting flat-shaped weekend temporal profiles, indicating minimal change in column throughout the weekend day (CalTech, Pico Rivera). These weekday-weekend differences are a fingerprint that can help identify the contribution of various NO₂ sources based on our understanding of their day-of-week variation (e.g., heavy duty diesel trucking, Harley et al., 2005) and important nonlinear chemical feedbacks (e.g, Valin et al., 2014).

In contrast to the order of magnitude difference in NO₂ between GeoTASO and OMPS in Seoul, South Korea (discussed in section 3.1), the near-nadir measurements over the LA Basin from OMPS on June 27th, 2017 (Figure 2b: $2-5 \times 10^{15}$ molecules cm⁻²) were much closer to the midday GeoTASO measurements during Raster 2 (median of 6.8×10^{15} molecules cm⁻²). The area covered by GeoTASO is approximately 1.5 times the area of a nadir OMPS pixel, but the GeoTASO raster does not encompass any single OMPS NM pixel in its entirety from this overpass in which to do a one-to-one comparison. However, the oversampled image (Figure 2d) does suggest that over a month-long timescale, OMPS NM observes NO₂ confined to the area measured by GeoTASO within the LA Basin at the same order of magnitude as this GeoTASO case study day.

4 Conclusions

This work illustrates the spatiotemporal detail that will be resolved with the upcoming GEO air quality measurements, using GeoTASO NO₂ retrievals as a proxy, and how ground-based and LEO datasets will play important roles in validating and connecting these GEO observations from the local- to global-scale. Data from GeoTASO, used as a testbed to address GEO validation needs and to anticipate future opportunities for air quality management applications, is used to resolve the spatiotemporal patterns of tropospheric column NO₂ over Seoul and Los Angeles. In the morning, under the influence of weak winds, spatial patterns of NO₂ reflect the spatial distribution of emission sources and topography over both the SMA and the LA Basin. NO₂ column densities over the SMA grow throughout the day as emission rates outweigh NO₂ removal from the column, while NO₂ in Los Angeles typically peaks during the mid-morning hours indicating that removal

processes overtake emission rates before midday. GEO observations will show whether these conclusions apply beyond the case studies shown here, as well as expanding to other metropolitan areas around the globe. These spatially and temporally refined measurements will begin to link the role of emissions and atmospheric dynamics with the spatial distribution of pollutants in regions impacted by poor air quality, details that past LEO observations were incapable of capturing.

In addition to the single days of GeoTASO data analyzed for each case study region, Pandora observations are used to demonstrate day-to-day and hour-to-hour variability of NO₂ that will be measured from GEO and provide a means of linking the satellite-based column measurements to variations in in situ surface concentrations. Over both the SMA and the LA Basin, Pandora measurements reveal that NO₂ columns vary between weekdays and weekends and between source and receptor sites. They also fluctuate greatly on a day-to-day basis from the statistically calculated diurnal averages, particularly near large sources. The frequent Pandora observations, many times per hour, and their anticipated co-location with surface air quality and meteorology monitoring instrumentation will also provide insight to transient local processes that better inform the use of column-integrated measurements for monitoring surface-based pollution.

LEO observations are now attaining similar spatial resolutions as those expected from the GEO instruments and are essential for intercalibrating radiances measured by each of the GEO instruments as well as cross-validating their data products. Observations from decades of LEO observations have provided compelling verification of multi-year changes in pollutant emissions in different regions of the world. However, as illustrated by these case studies, pollutant concentrations vary greatly through the day, particularly in urban areas. Variations are driven by factors that also change through the day: emissions, photochemistry, and meteorology. Sparse observations, including temporally sparse LEO observations (e.g. OMPS) and spatially sparse surface measurements (e.g. Pandora), do not permit these factors to be disentangled, limiting improvements in air quality assessment and prediction. The GeoTASO data shown in these case studies illustrate one change in perspective the GEO observations will provide: moving beyond coarse, static early-afternoon snapshots from LEO to dynamic visualization of chemical weather. Together the pieces of this system will enable better understanding of the locations and magnitudes of emissions and of meteorological influences, better monitoring of the air we breathe, and ultimately more effective strategies for improving air quality.

Acknowledgements

The authors extend appreciation to the South Coast Air Quality Monitoring District (SCAQMD) and our colleagues at UCLA and CalTech for providing accommodations for the Pandora Spectrometers in the LA Basin, Olga Pikel'naya for providing high temporal resolution SCAQMD in situ meteorology data, the KORUS-AQ science team, Nader Abuhassan and NASA's Pandora Project, ESA's Pandonia team, NASA SARP 2017 and NSRC, Barry Lefer from NASA Headquarters for inviting us to participate in SARP 2017, and our pilots and flight crew during both field missions.

7 Funding

This work was partly funded by EPA National Exposure Research Laboratory and NASA Earth Science Division's GEO-CAPE Mission Study and Tropospheric Composition Program.

Pandora deployment, operation and the near real time processing of data were collaboratively supported by the NASA Earth Science Division funded Pandora Project team (R. Swap, PI) at GSFC in Greenbelt, MD, USA and by the ESA funded Pandonia team (A. Cede, PI) from Luftblick in Kreith, Austria.

Laura Judd's research was supported by an appointment to the NASA Postdoctoral Program at the NASA Langley Research Center, administered by Universities Space Research Association under contract with NASA.

References

- Banta RM, Senff CJ, Nielsen-Gammon J, Darby LS, Ryerson TB, Alvarez RJ, et al. (2005). A bad air day in Houston. *Bulletin of the American Meteorological Society* 86, 657–669.
- Beirle S, Platt U, Wenig M, and Wagner T (2003). Weekly cycle of NO₂ by GOME measurements: A signature of anthropogenic sources. *Atmospheric Chemistry and Physics Discussions* 3, 3451–3467. doi:10.5194/acpd-3-3451-2003.
- Beirle S, Boersma KF, Platt U, Lawrence MG, and Wagner T (2011). Megacity Emissions and Lifetimes of Nitrogen Oxides Probed from Space. *Science* 333, 1737–1739. doi:10.1126/science.1207824. [PubMed: 21940891]
- Boersma KF, Eskes HJ, and Brinkma EJ (2004). Error analysis for tropospheric NO₂ retrieval from space. *Journal of Geophysical Research: Atmospheres* 109, doi:10.1029/2003JD003962.
- Boersma KF, Jacob DJ, Trainic M, Rudich Y, DeSmedt I, Dirksen R, et al. (2009). Validation of urban NO₂ concentrations and their diurnal and seasonal variations observed from the SCIAMACHY and OMI sensors using in situ surface measurements in Israeli cities. *Atmospheric Chemistry and Physics* 9, 3867–3879. doi:10.5194/acp-9-3867-2009.
- Bovensmann H, Burrows JP, Buchwitz M, Frerick J, Noel S, Rozanov VV, et al. (1999). SCIAMACHY: Mission objectives and measurement modes. *Journal of the atmospheric sciences* 56, 127–150.
- Brocardo S, Heue K-P, Walter D, Meyer C, Kokhanovsky A, v. d. A R, et al. (2017). Intra-pixel variability in satellite tropospheric NO₂ column densities derived from simultaneous spaceborne and airborne observations. *Atmospheric Measurement Techniques Discussions*, 1–32. doi:10.5194/amt-2016-366.
- Bucsela EJ, Perring AE, Cohen RC, Boersma KF, Celarier EA, Gleason JF, et al. (2008). Comparison of tropospheric NO₂ from in situ aircraft measurements with near-real-time and standard product data from OMI. *Journal of Geophysical Research* 113. doi:10.1029/2007JD008838.
- Bucsela EJ, Krotkov NA, Celarier EA, Lamsal LN, Swartz WH, Bhartia PK, et al. (2013). A new stratospheric and tropospheric NO₂ retrieval algorithm for nadir-viewing satellite instruments: applications to OMI. *Atmos. Meas. Tech* 6, 2607–2626. doi:10.5194/amt-6-2607-2013.
- Burrows JP, Weber M, Buchwitz M, Rozanov V, Ladstätter-Weissenmayer A, Richter A, et al. (1999). The global ozone monitoring experiment (GOME): Mission concept and first scientific results. *Journal of the Atmospheric Sciences* 56, 151–175.
- Callies J, Corpaccioli E, Eisinger M, Hahne A, and Lefebvre A (2000). GOME-2-Metop's second-generation sensor for operational ozone monitoring. *ESA bulletin* 102, 28–36.
- CEOS (2011). A Geostationary Satellite Constellation for Observing Global Air Quality: An International Path Forward. Available at: http://ceos.org/document_management/Virtual_Constellations/ACC/Documents/AC-VC_Geostationary-Cx-for-Global-AQ-final_Apr2011.pdf [Accessed March 6, 2018].
- Cohan DS, Hu Y, and Russell AG (2006). Dependence of ozone sensitivity analysis on grid resolution. *Atmospheric Environment* 40, 126–135. doi:10.1016/j.atmosenv.2005.09.031.
- Crawford JH, Al-Saadi J, Pierce G, Long RW, Szykman JJ, Leitch J, et al. (2016). Multi-perspective observations of NO₂ over the Denver area during DISCOVER-AQ: Insights for Future Monitoring. *EM: Air and Waste Management Associations Magazine for Environmental Managers*, 5.
- Dancaert T, Fayt C, Van Roozendaal M, De Smedt I, Letocart V, Merlaud A, et al. (2017). QDOAS Software User Manual. Available at: http://uv-vis.aeronomie.be/software/QDOAS/QDOAS_manual.pdf [Accessed March 27th, 2018].
- de Foy B, Krotkov NA, Bei N, Herndon SC, Huey LG, Martinez A-P, et al. (2009). Hit from both sides: tracking industrial and volcanic plumes in Mexico City with surface measurements and OMI

- SO₂ retrievals during the MILAGRO field campaign. *Atmospheric Chemistry and Physics* 9, 9599–9617. doi:10.5194/acp-9-9599-2009.
- de Foy B, Lu Z, Streets DG, Lamsal LN, and Duncan BN (2015). Estimates of power plant NO_x emissions and lifetimes from OMI NO₂ satellite retrievals. *Atmospheric Environment* 116, 1–11. doi:10.1016/j.atmosenv.2015.05.056.
- de Foy B, Lu Z, and Streets DG (2016). Impacts of control strategies, the Great Recession and weekday variations on NO₂ columns above North American cities. *Atmospheric Environment* 138, 74–86. doi:10.1016/j.atmosenv.2016.04.038.
- De Smedt I, Stavrou T, Hendrick F, Danckaert T, Vlemmix T, Pinardi G, et al. (2015). Diurnal, seasonal and long-term variations of global formaldehyde columns inferred from combined OMI and GOME-2 observations. *Atmospheric Chemistry and Physics Discussions* 15, 12241–12300. doi:10.5194/acpd-15-12241-2015.
- Duncan BN, Yoshida Y, Olson JR, Sillman S, Martin RV, Lamsal L, et al. (2010). Application of OMI observations to a space-based indicator of NO_x and VOC controls on surface ozone formation. *Atmospheric Environment* 44, 2213–2223. doi:10.1016/j.atmosenv.2010.03.010.
- Duncan BN, Prados AI, Lamsal LN, Liu Y, Streets DG, Gupta P, et al. (2014). Satellite data of atmospheric pollution for U.S. air quality applications: Examples of applications, summary of data end-user resources, answers to FAQs, and common mistakes to avoid. *Atmospheric Environment* 94, 647–662. doi:10.1016/j.atmosenv.2014.05.061.
- Duncan BN, Lamsal LN, Thompson AM, Yoshida Y, Lu Z, Streets DG, et al. (2016). A space-based, high-resolution view of notable changes in urban NO_x pollution around the world (2005–2014). *Journal of Geophysical Research: Atmospheres* 121, 976–996. doi:10.1002/2015JD024121.
- Fishman J, Iraci LT, Al-Saadi J, Chance K, Chavez F, Chin M, et al. (2012). The United States' Next Generation of Atmospheric Composition and Coastal Ecosystem Measurements: NASA's Geostationary Coastal and Air Pollution Events (GEO-CAPE) Mission. *Bulletin of the American Meteorological Society* 93, 1547–1566. doi:10.1175/BAMS-D-11-00201.1.
- Flynn CM, Pickering KE, Crawford JH, Lamsal L, Krotkov N, Herman J, et al. (2014). Relationship between column-density and surface mixing ratio: Statistical analysis of O₃ and NO₂ data from the July 2011 Maryland DISCOVER-AQ mission. *Atmospheric Environment* 92, 429–441. doi:10.1016/j.atmosenv.2014.04.041.
- Flynn LE, Homstein J, and Hilsenrath E (2004). The ozone mapping and profiler suite (OMPS). The next generation of US ozone monitoring instruments. in *IGARSS 2004. 2004 IEEE International Geoscience and Remote Sensing Symposium*, 155. doi:10.1109/IGARSS.2004.1368968.
- Goldberg DL, Lamsal LN, Loughner CP, Swartz WH, Lu Z, and Streets DG (2017). A high-resolution and observationally constrained OMI NO₂ satellite retrieval. *Atmospheric Chemistry and Physics* 17, 11403–11421. doi:10.5194/acp-17-11403-2017.
- Harley RA, Marr LC, Lehner JK, and Giddings SN (2005). Changes in Motor Vehicle Emissions on Diurnal to Decadal Time Scales and Effects on Atmospheric Composition. 7. *Environmental Science & Technology*.
- Herman J, Cede A, Spinei E, Mount G, Tzortziou M, and Abuhassan N (2009). NO₂ column amounts from ground-based Pandora and MFDOAS spectrometers using the direct-sun DOAS technique: Intercomparisons and application to OMI validation. *Journal of Geophysical Research* 114. doi:10.1029/2009JD011848.
- Herman J, Evans R, Cede A, Abuhassan N, Petropavlovskikh I, and McConville G (2015). Comparison of ozone retrievals from the Pandora spectrometer system and Dobson spectrophotometer in Boulder, Colorado. *Atmospheric Measurement Techniques* 8, 3407–3418. doi:10.5194/amt-8-3407-2015.
- IGACO (2004). International Global Atmospheric Chemistry Observations Strategy Theme Report. (No. ESA SP-1282, GW No. 159, WMO TD No. 1235). Available at: <http://www.fao.org/gtos/igos/docs/IGACO-Theme-Report-2004-4.pdf> [Accessed March 6, 2018].
- Ingmann P, Veihelmann B, Langen J, Lamarre D, Stark H, and Courrèges-Lacoste GB (2012). Requirements for the GMES Atmosphere Service and ESA's implementation concept: Sentinels-4/-5 and -5p. *Remote Sensing of Environment* 120, 58–69. doi:10.1016/j.rse.2012.01.023.

- Irie H, Kanaya Y, Akimoto H, Tanimoto H, Wang Z, Gleason JF, et al. (2008). Validation of OMI tropospheric NO₂ column data using MAX-DOAS measurements deep inside the North China Plain in June 2006: Mount Tai Experiment 2006. *Atmospheric Chemistry and Physics* 8, 6577–6586. doi:10.5194/acp-8-6577-2008.
- Jaegle L, Steinberger L, Martin RV, and Chance K (2005). Global partitioning of NO_x sources using satellite observations: Relative roles of fossil fuel combustion, biomass burning and soil emissions. *Faraday Discussions* 130, 407. doi:10.1039/b502128f. [PubMed: 16161795]
- Janjic Z, and Gall R (2012). Scientific documentation of the NCEP nonhydrostatic multiscale model on the B grid (NMMB). Part 1 Dynamics. UCAR/NCAR doi:10.5065/D6WH2MZX.
- Jin X, Fiore AM, Murray LT, Valin LC, Lamsal LN, Duncan B, et al. (2017). Evaluating a Space-Based Indicator of Surface Ozone-NO_x-VOC Sensitivity Over Midlatitude Source Regions and Application to Decadal Trends: Space-Based Indicator of O₃ Sensitivity. *Journal of Geophysical Research: Atmospheres* 122, 10,439–10,461. doi:10.1002/2017JD026720.
- Judd LM (2016). Investigating the spatiotemporal variability of NO₂ and photochemistry in urban areas Dissertation. Houston, TX: University of Houston.
- Kim J, Kim M, and Choi M (2017). “Monitoring Aerosol Properties in East Asia from Geostationary Orbit: GOCI, MI and GEMS,” in *Air Pollution in Eastern Asia: An Integrated Perspective ISSI Scientific Report Series*. (Springer, Cham), 323–333. doi:10.1007/978-3-319-59489-7_15.
- Kim S-W, Heckel A, McKeen SA, Frost GJ, Hsie E-Y, Trainer MK, et al. (2006). Satellite-observed U.S. power plant NO_x emission reductions and their impact on air quality. *Geophysical Research Letters* 33. doi:10.1029/2006GL027749.
- Kleist DT, and Ide K (2015a). An OSSE-Based Evaluation of Hybrid Variational-Ensemble Data Assimilation for the NCEP GFS. Part I: System Description and 3D-Hybrid Results. *Monthly Weather Review* 143, 433–451. doi:10.1175/MWR-D-13-00351.1.
- Kleist DT, and Ide K (2015b). An OSSE-Based Evaluation of Hybrid Variational-Ensemble Data Assimilation for the NCEP GFS. Part II: 4D-EnVar and Hybrid Variants. *Monthly Weather Review* 143, 452–470. doi:10.1175/MWR-D-13-00350.1.
- Knepp T, Pippin M, Crawford J, Chen G, Szykman J, Long R, et al. (2015). Estimating surface NO₂ and SO₂ mixing ratios from fast-response total column observations and potential application to geostationary missions. *Journal of Atmospheric Chemistry* 72, 261–286. doi:10.1007/s10874-013-9257-6. [PubMed: 26692593]
- Krotkov NA, Lamsal LN, Celarier EA, Swartz WH, Marchenko SV, Bucsela EJ, et al. (2017). The version 3 OMI NO₂ standard product. *Atmospheric Measurement Techniques* 10, 3133–3149. doi:10.5194/amt-10-3133-2017.
- Lamsal LN, Martin RV, van Donkelaar A, Celarier EA, Bucsela EJ, Boersma KF, et al. (2010). Indirect validation of tropospheric nitrogen dioxide retrieved from the OMI satellite instrument: Insight into the seasonal variation of nitrogen oxides at northern midlatitudes. *Journal of Geophysical Research* 115. doi:10.1029/2009JD013351.
- Lamsal LN, Janz SJ, Krotkov NA, Pickering KE, Spurr RJD, Kowalewski MG, et al. (2017). High-resolution NO₂ observations from the Airborne Compact Atmospheric Mapper: Retrieval and validation: High-Resolution NO₂ Observations. *Journal of Geophysical Research: Atmospheres* 122, 1953–1970. doi:10.1002/2016JD025483.
- Leitch JW, Delker T, Good W, Ruppert L, Murcray F, Chance K, et al. (2014). The GeoTASO airborne spectrometer project. doi:10.1117/12.2063763.
- Levelt PF, Oord GHJ, Dobber van den, Malkki MR, Visser A, Vries H, de J, et al. (2006). The ozone monitoring instrument. *IEEE Transactions on Geoscience and Remote Sensing* 44, 1093–1101. doi:10.1109/TGRS.2006.872333.
- Liang J, Horowitz LW, Jacob DJ, Wang Y, Fiore AM, Logan JA, et al. (1998). Seasonal budgets of reactive nitrogen species and ozone over the United States, and export fluxes to the global atmosphere. *J. Geophys. Res* 103, 13435–13450. doi:10.1029/97JD03126.
- Martin RV (2003). Global inventory of nitrogen oxide emissions constrained by space-based observations of NO₂ columns. *Journal of Geophysical Research* 108. doi:10.1029/2003JD003453.

- Martin RV, Fiore AM, and Van Donkelaar A (2004). Space-based diagnosis of surface ozone sensitivity to anthropogenic emissions. *Geophysical Research Letters* 31. doi: 10.1029/2004GL019416.
- McLinden CA, Fioletov V, Boersma KF, Krotkov N, Sioris CE, Veefkind JP, et al. (2012). Air quality over the Canadian oil sands: A first assessment using satellite observations. *Geophysical Research Letters* 39, n/a-n/a. doi:10.1029/2011GL050273.
- National Academies of Sciences, Engineering, and Medicine (2018). *Thriving on Our Changing Planet: A Decadal Strategy for Earth Observation from Space*. Washington, DC: The National Academies Press <https://doi.org/10.17226/24938>.
- Nowlan CR, Liu X, Leitch JW, Chance K, Gonzalez Abad G, Liu C, et al. (2016). Nitrogen dioxide observations from the Geostationary Trace gas and Aerosol Sensor Optimization (GeoTASO) airborne instrument: Retrieval algorithm and measurements during DISCOVER-AQ Texas 2013. *Atmospheric Measurement Techniques* 9, 2647–2668. doi:10.5194/amt-9-2647-2016.
- Palmer PI, Jacob DJ, Chance K, Martin RV, Spurr RJD, Kurosu TP, et al. (2001). Air mass factor formulation for spectroscopic measurements from satellites: Application to formaldehyde retrievals from the Global Ozone Monitoring Experiment. *J. Geophys. Res* 106, 14539–14550. doi: 10.1029/2000JD900772.
- Richter A, Burrows J, Nüss H, Granier C, and Niemeier U (2005). Increase in tropospheric nitrogen dioxide over China observed from space. *Nature* 437, 129–32. doi:10.1038/nature04092. [PubMed: 16136141]
- Russell AR, Valin LC, Bucsela EJ, Wenig MO, and Cohen RC (2010). Space-based Constraints on Spatial and Temporal Patterns of NO_x Emissions in California, 2005–2008. *Environmental Science & Technology* 44, 3608–3615. doi:10.1021/es903451j. [PubMed: 20364869]
- Russell AR, Perring AE, Valin LC, Bucsela EJ, Browne EC, Wooldridge PJ, et al. (2011). A high spatial resolution retrieval of NO_2 column densities from OMI: method and evaluation. *Atmospheric Chemistry and Physics* 11, 8543–8554. doi:10.5194/acp-11-8543-2011.
- Russell AR, Valin LC, and Cohen RC (2012). Trends in OMI NO_2 observations over the United States: effects of emission control technology and the economic recession. *Atmospheric Chemistry and Physics* 12, 12197–12209. doi:10.5194/acp-12-12197-2012.
- Schroeder JR, Crawford JH, Fried A, Walega J, Weinheimer A, Wisthaler A, et al. (2017). New insights into the column $\text{CH}_2\text{O}/\text{NO}_2$ ratio as an indicator of near-surface ozone sensitivity: $\text{CH}_2\text{O}/\text{NO}_2$ as Indicator of O_3 Sensitivity. *Journal of Geophysical Research: Atmospheres* 122, 8885–8907. doi:10.1002/2017JD026781.
- SEDAC (NASA Socioeconomic Data and Applications Center) Center for International Earth Science Information Network - CIESIN - Columbia University, and Information Technology Outreach Services - ITOS - University of Georgia 2013 Global Roads Open Access Data Set, Version 1 (gROADSv1). Palisades, NY: NASA Socioeconomic Data and Applications Center (SEDAC)10.7927/H4VD6WCT. [Accessed March 18, 2018].
- Sussmann R, Stremme W, Burrows JP, Richter A, Seiler W, and Rettinger M (2005). Stratospheric and tropospheric NO_2 variability on the diurnal and annual scale: a combined retrieval from ENVISAT/SCIAMACHY and solar FTIR at the Permanent Ground-Truthing Facility Zugspitze/Garmisch. *Atmospheric Chemistry and Physics* 5, 2657–2677.
- Travis KR, Jacob DJ, Fisher JA, Kim PS, Marais EA, Zhu L, et al. (2016). Why do models overestimate surface ozone in the Southeast United States? *Atmospheric Chemistry and Physics* 16, 13561–13577. doi:10.5194/acp-16-13561-2016. [PubMed: 29619045]
- Tzortziou M, Herman JR, Cede A, Loughner CP, Abuhassan N, and Naik S (2015). Spatial and temporal variability of ozone and nitrogen dioxide over a major urban estuarine ecosystem. *Journal of Atmospheric Chemistry* 72, 287–309. doi:10.1007/s10874-013-9255-8.
- Valin LC, Russell AR, Hudman RC, and Cohen RC (2011a). Effects of model resolution on the interpretation of satellite NO_2 observations. *Atmospheric Chemistry and Physics* 11, 11647–11655. doi:10.5194/acp-11-11647-2011.
- Valin LC, Russell AR, Bucsela EJ, Veefkind JP, and Cohen RC (2011b). Observation of slant column NO_2 using the super-zoom mode of AURA-OMI. *Atmospheric Measurement Techniques Discussions* 4, 1989–2005. doi:10.5194/amtd-4-1989-2011.

- Valin LC, Russell AR, and Cohen RC (2013). Variations of OH radical in an urban plume inferred from NO₂ column measurements. *Geophysical Research Letters* 40, 1856–1860. doi:10.1002/grl.50267.
- Valin LC, Russell AR, and Cohen RC (2014). Chemical feedback effects on the spatial patterns of the NO_x weekend effect: a sensitivity analysis. *Atmospheric Chemistry and Physics Discussions* 13, 19173–19192. doi:10.5194/acpd-13-19173-2013.
- van der A RJ, Eskes HJ, Boersma KF, van Noije TPC, Van Roozendaal M, De Smedt I, et al. (2008). Trends, seasonal variability and dominant NO_x source derived from a ten year record of NO₂ measured from space. *Journal of Geophysical Research* 113. doi:10.1029/2007JD009021.
- van Geffen JHG, Boersma KF, Eskes HJ, Maasakkers JD, and Veefkind JP (2017). TROPOMI ATBD of the total and tropospheric NO₂ data products. KNMI Available at: http://www.tropomi.eu/sites/default/files/files/S5P-KNMI-L2-0005-RP-TROPOMI_ATBD_NO2_data_products-v1p1p0-20170816_signed.pdf [Accessed January 16, 2018].
- Veefkind JP, Aben I, McMullan K, Forster H, de Vries J, Otter G, et al. (2012). TROPOMI on the ESA Sentinel-5 Precursor: A GMES mission for global observations of the atmospheric composition for climate, air quality and ozone layer applications. *Remote Sensing of Environment* 120, 70–83. doi: 10.1016/j.rse.2011.09.027.
- Yang K, Carn SA, Ge C, Wang J, and Dickerson RR (2014). Advancing measurements of tropospheric NO₂ from space: New algorithm and first global results from OMPS. *Geophysical Research Letters* 41, 4777–4786. doi:10.1002/2014GL060136.
- Zhou Y, Brunner D, Spurr RJD, Boersma KF, Sneep M, Popp C, et al. (2010). Accounting for surface reflectance anisotropy in satellite retrievals of tropospheric NO₂. *Atmospheric Measurement Techniques Discussions* 3, 1971–2012. doi:10.5194/amtd-3-1971-2010.
- Zhu L, Jacob DJ, Mickley LJ, Marais EA, Cohan DS, Yoshida Y, et al. (2014). Anthropogenic emissions of highly reactive volatile organic compounds in eastern Texas inferred from oversampling of satellite (OMI) measurements of HCHO columns. *Environmental Research Letters* 9, 114004. doi:10.1088/1748-9326/9/11/114004.
- Zhu L, Jacob DJ, Keutsch FN, Mickley LJ, Scheffe R, Strum M, et al. (2017). Formaldehyde (HCHO) As a Hazardous Air Pollutant: Mapping Surface Air Concentrations from Satellite and Inferring Cancer Risks in the United States. *Environmental Science & Technology* 51, 5650–5657. doi: 10.1021/acs.est.7b01356. [PubMed: 28441488]
- Zoogman P, Liu X, Suleiman RM, Pennington WF, Flittner DE, Al-Saadi JA, et al. (2017). Tropospheric emissions: Monitoring of pollution (TEMPO). *Journal of Quantitative Spectroscopy and Radiative Transfer* 186, 17–39. doi:10.1016/j.jqsrt.2016.05.008.

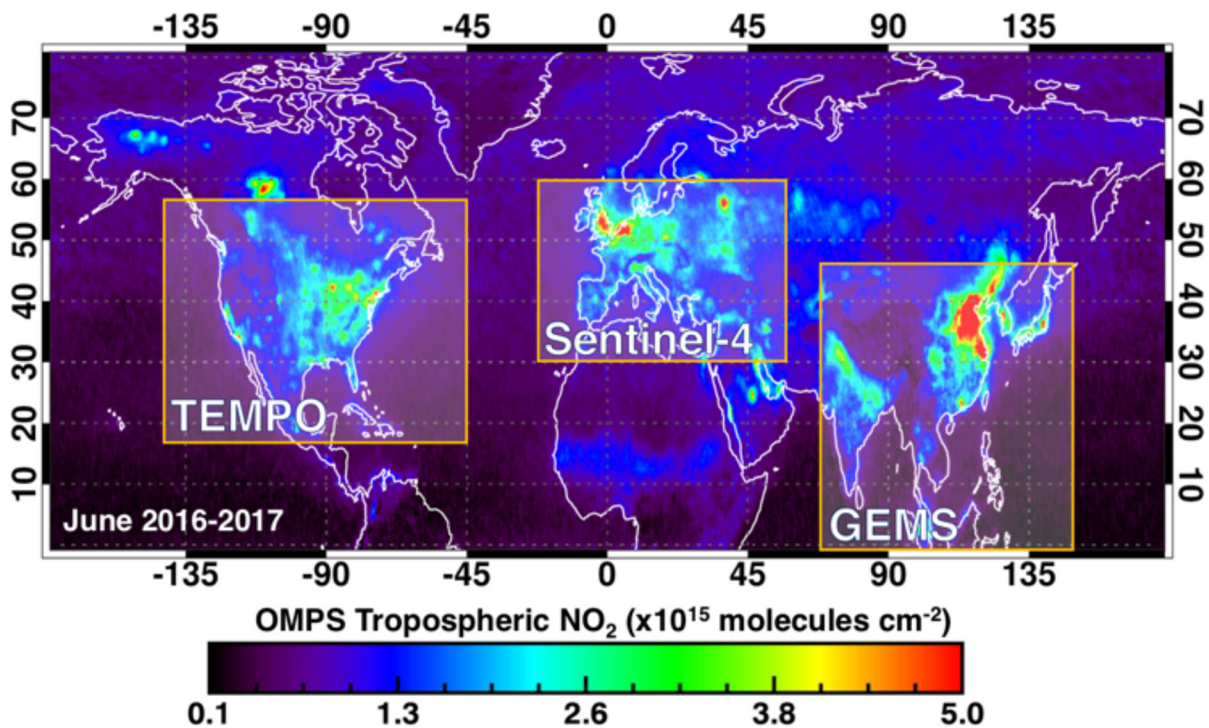


Figure 1:
 Global map of OMPS tropospheric NO₂ vertical columns for June 2016 and June 2017 averaged to 0.25° × 0.25° with the overlaid approximate spatial coverages of the planned geostationary platforms: TEMPO over North America, Sentinel-4 over Europe, and GEMS over East Asia.

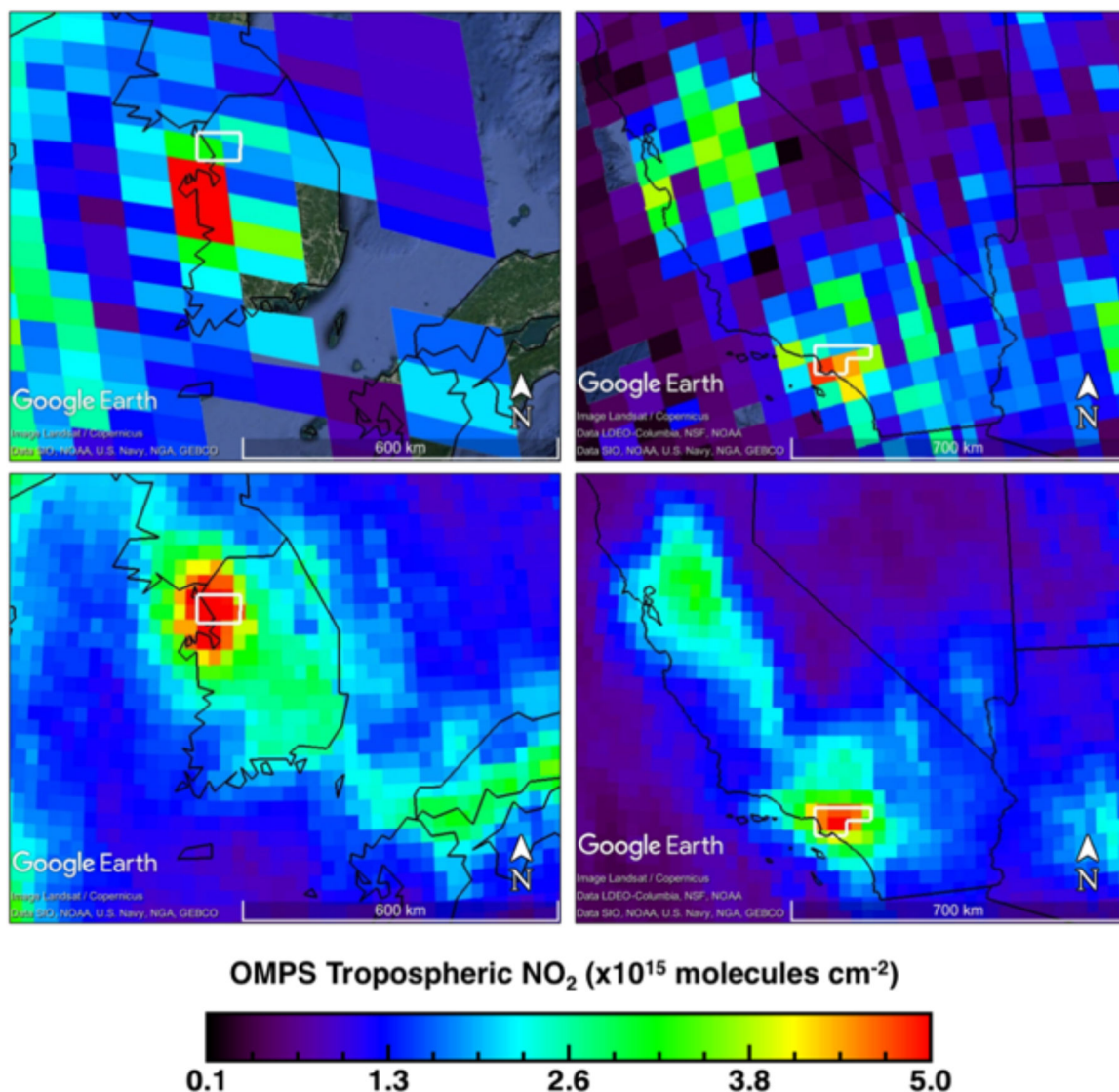


Figure 2: Tropospheric NO₂ data from OMPS aboard Suomi-NPP for single overpasses on (a) June 9th 2016 over South Korea and (b) June 27th, 2017 over California. The monthly averaged 0.25° × 0.25° tropospheric NO₂ from OMPS is shown for (c) June 2016 over South Korea and (d) June 2017 over California. White polygons in each map outline the area of the GeoTASO flights.



Figure 3:

Maps of (a) the Seoul Metropolitan Area (SMA) and (b) the Los Angeles Basin. Major roads (SEDAC, 2013) are drawn in red (I-5, I-10, and CA-60 are outlined in blue in Panel b). Pandora sites are labeled with white star icons, and regions discussed in the paper labeled in yellow. The green triangle in the SMA is Mount Gwanaksan, and the airplane icon in Los Angeles depicts the location of LAX Airport. GeoTASO rasters cover the approximate area depicted by the white polygons.

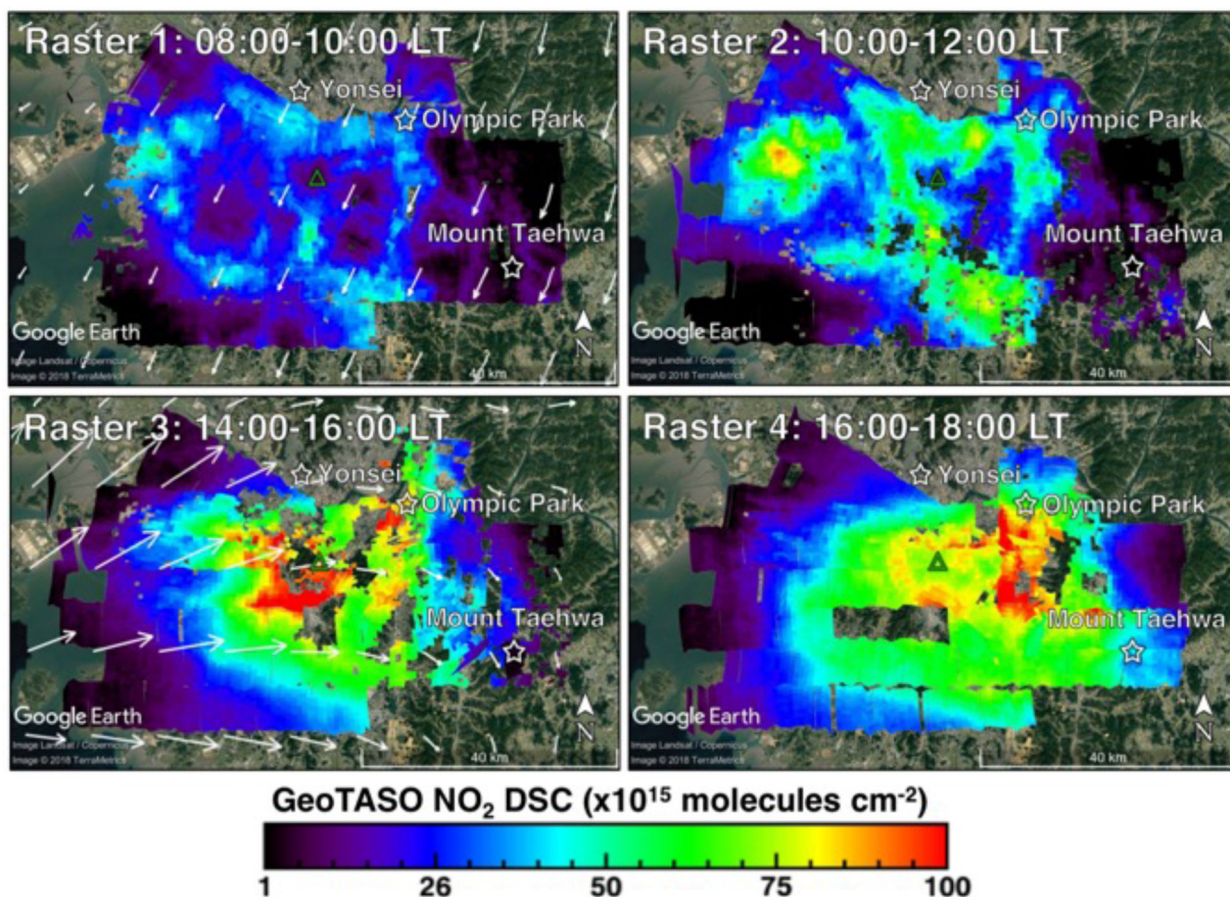


Figure 4: Maps of GeoTASO NO₂ DSCs over SMA on June 9th, 2016 for (a) Raster 1 from 08:00–10:00 LT, (b) Raster 2 from 10:00–12:00 LT, (c) Raster 3 from 14:00–16:00 LT, and (d) Raster 4 from 16:00–18:00 LT. Pandora sites are labeled with white star icons. Rasters 1 and 3 includes wind vectors averaged through the lowest 500 m agl from the full resolution Global Data Assimilation System (GDAS) at (a) 00:00 UTC (09:00 LT) and (c) 06:00 UTC (15:00 LT).

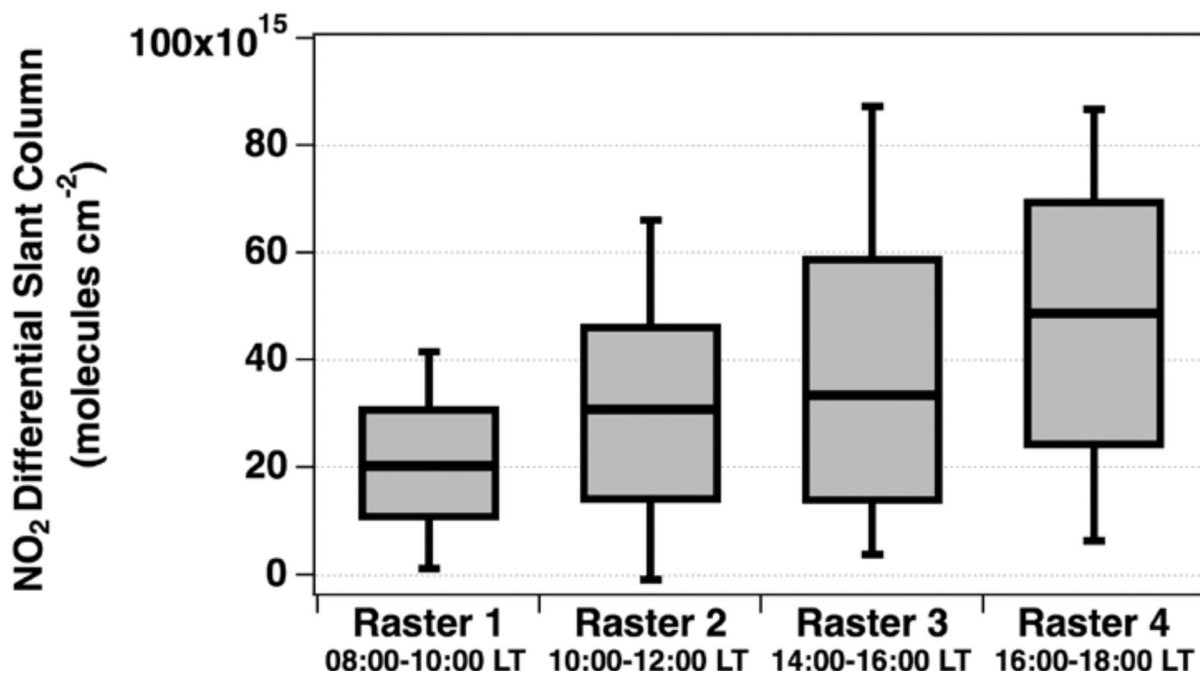


Figure 5: Box plots showing the percentile distributions of NO₂ DSCs for each Raster in SMA from Figure 4. The shaded box shows 25th–75th percentile range with the whiskers extending to the 5th and 95th percentiles. The solid line dividing each shaded box is the median.

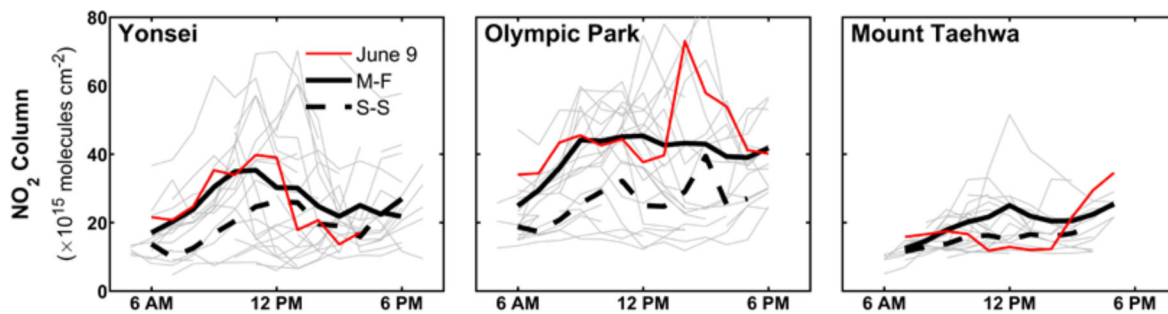


Figure 6:

Hourly averaged NO₂ vertical columns observed by ground-based Pandora spectrometers at Yonsei University, Olympic Park, and Mount Taehwa. Grey lines are the individual day diurnal averages from May 5th through June 15th, 2016. June 9th, 2016 is overlaid in red, the weekday (Monday-Friday) averages are the black solid lines, and weekend (Saturday-Sunday) average observations are the black dashed lines.

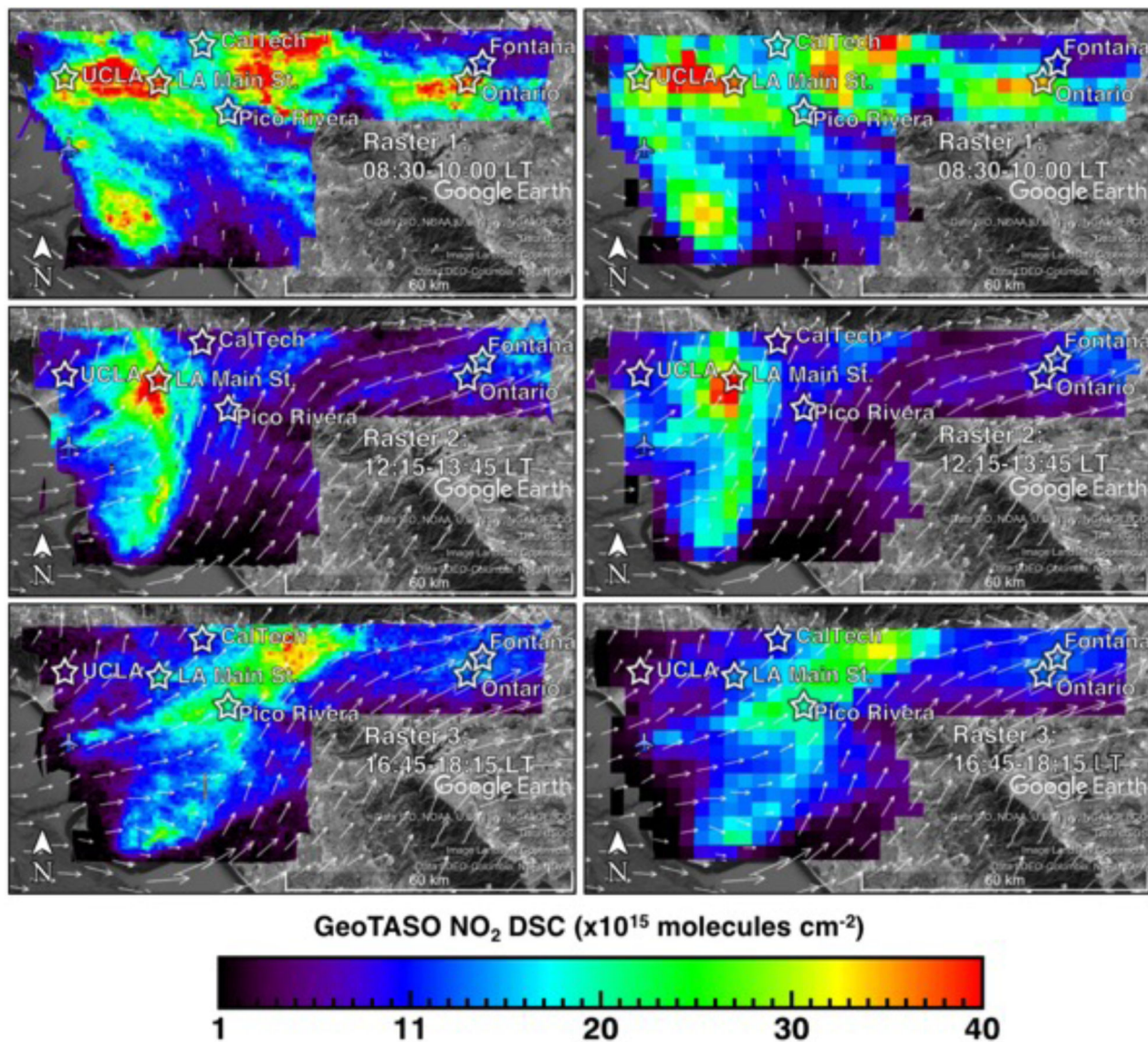


Figure 7: Maps of GeoTASO NO₂ DSCs over the LA Basin on June 27th, 2017. Raster 1 from 08:30–10:00 LT is shown in a and b, Raster 2 from 12:15–13:45 LT is shown in c and d, and Raster 3 from 16:45–18:15 LT is shown in e and f. Panels a, c, and e are at 750 m × 750 m resolution, whereas b, d, and f are the DSCs binned to 3 km × 3 km spatial resolution. Overlaid are the boundary layer averaged wind vectors from the NAM-CONUS 3-km nest analysis for 16:00 UTC (09:00 LT) in a and b, 20:00 UTC (13:00 LT) in c and d, and 00:00 UTC (17:00 LT) in e and f.

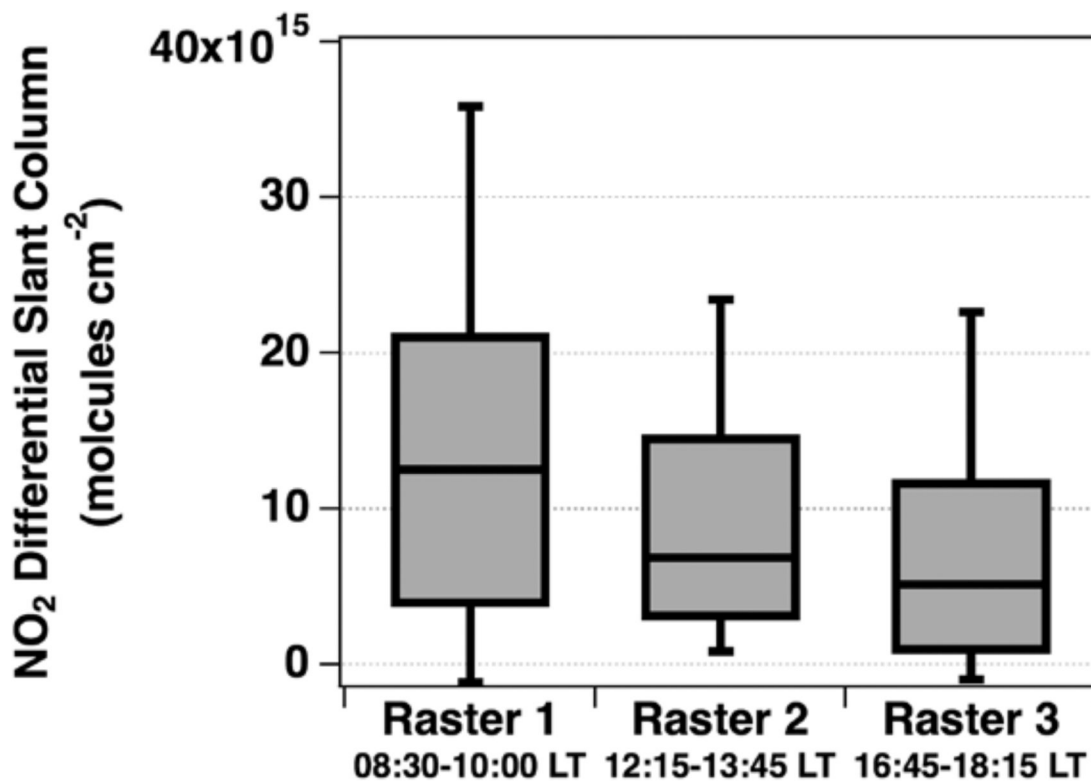


Figure 8: Box plots showing the percentile distributions of NO₂ DSCs for each raster in the LA Basin from Figure 7. The shaded box shows 25th–75th percentile range with the whiskers extending to the 5th and 95th percentiles. The solid line dividing each shaded box is the median.

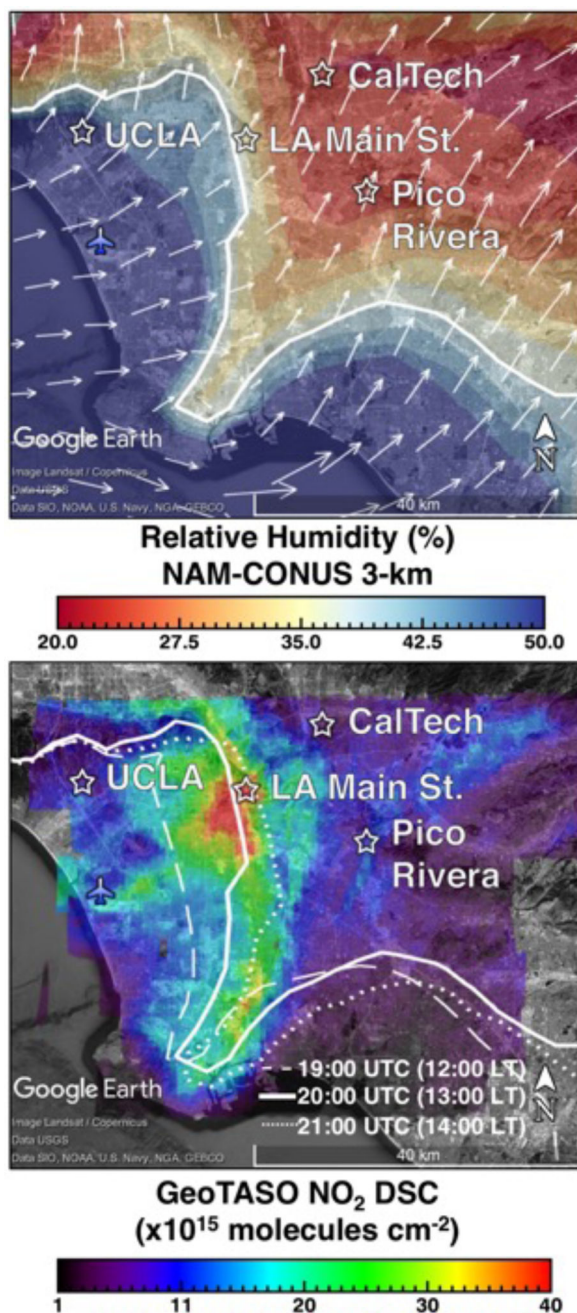


Figure 9:
 (a) Relative humidity from the NAM-CONUS 3-km nest at 20:00 UTC (13:00 LT) with overlaid modeled boundary layer averaged wind vectors and a white contour at 40% relative humidity boundary indicating the sea breeze front position and (b) NO₂ DSCs over the western side of the LA Basin during Raster 2 with the indicated sea breeze front position identified from the NAM-CONUS 3-km nest 40% relative humidity contour at 19:00UTC (long dashes: 12:00 LT), 20:00UTC (solid: 13:00 LT) and 21:00UTC (dotted: 14:00 LT).

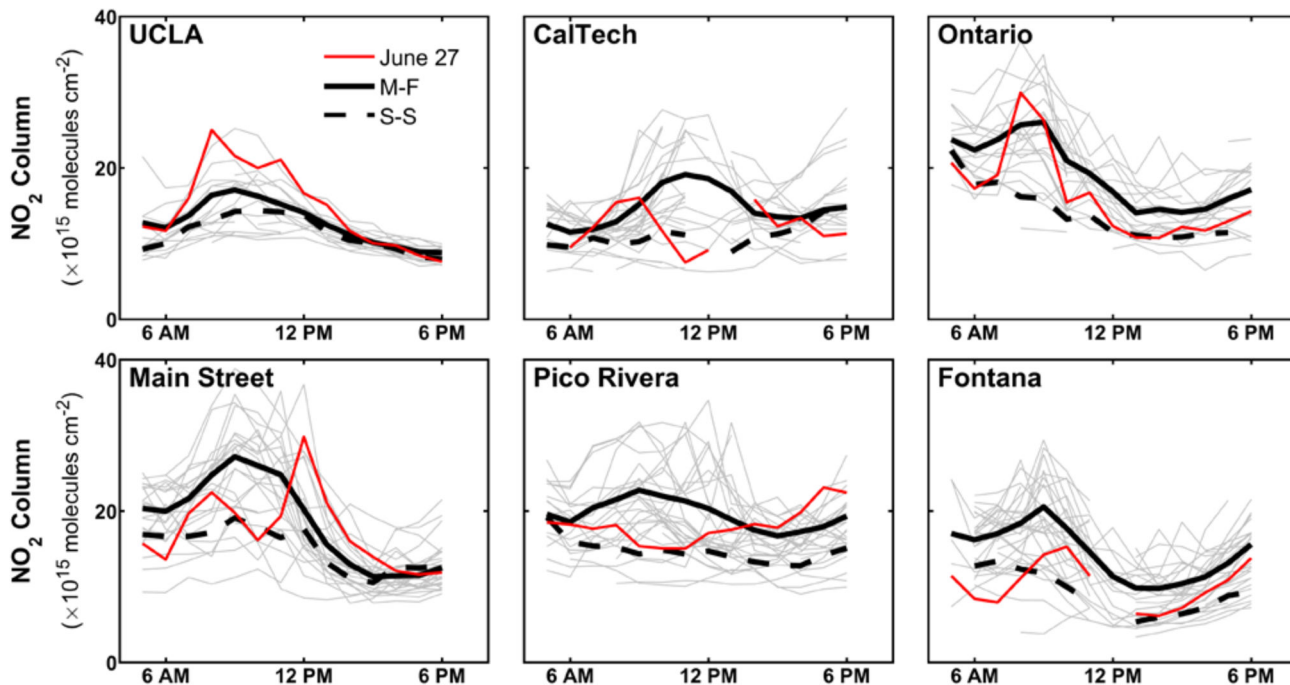


Figure 10. Hourly averaged NO₂ vertical columns observed by ground-based Pandora spectrometers at UCLA, Los Angeles Main Street, CalTech, Pico Rivera, Ontario and Fontana. Grey lines are the individual day diurnal averages from June 15th through July 15th, 2017. June 27th, 2016 is overlaid in red, the weekday (Monday-Friday) averages are the black solid lines, and weekend (Saturday-Sunday) average observations are the black dashed lines.